Ink-Jet Printing and Electrodeposition for the Production of Free Standing and Polymer Supported Micronet Electrodes

A. V. Oriani,[a,*,z] M. A. Spreafico,[a] F. Pedroli,[a] A. Marrani,[b] I. Falco,[b] P. Cojocaru,[b,] F. Triulzi,[b] M. Apostolo,[b] and L. Magagnin[a,**]**

[a]Dipartimento di Chimica, Materiali e Ingegneria Chimica "Giulio Natta", Politecnico di Milano, 20131 Milano, Italy [b]Solvay Specialty Polymers, Alternative Energy R&D, 20021 Bollate (MI), Italy

Manuscript submitted December 9, 2014; revised manuscript received December 26, 2014. Published January 9, 2015.

Transparent conductive electrodes (TCEs) are widely used in the growing market of organic and thin film solar cells, liquid crystalline displays and O-LEDs.[1–3] A common requirement among these applications is the possibility of producing transparent and conductive electrodes directly on polymeric substrates, which is related to the growing interest in flexible electronics. Indium tin oxide (ITO), the most commonly used material in the display industry, has several limitations when considering the actual needs in this field: it is prone to cracking on flexible substrates,[4,5] it is expensive, due to the presence of Indium, and requires high temperatures during the thin film fabrication process.[6] Therefore substitution of ITO is necessary to satisfy the evolution of electronic industry; at the moment attention is mainly focused on conductive polymers,[4,7,8] single-walled carbon nanotubes (SWNTs),[9–11] graphene and metallic nanostructures.[12–15] If polymeric transparent electrodes are limited by their intrinsic low conductivity, carbon nanotubes and silver nanowires (AgNW) show promising properties but still need some improvement. Transparent conducting electrodes produced with SWNTs have typical resistance of 200 Ω/□ at 80% transmission (at a wavelength of 550 nm).[11] This resistance value is an order of magnitude higher than that of ITO, therefore it is insufficient for applications in large-area devices. Lower sheet resistance may be obtained with AgNW, due to the intrinsically lower resistivity of silver, but issues are relative to the presence of height variations greater than 100 nm in the deposit.[16–19] Despite their promising properties as potential replacements for ITO, these materials still suffer from the trade-off between electrical conductivity and light transmission characteristics. To increase electrical conductivity thicker layers are needed, but this enhancement comes at the expenses of optical transmittance and vice versa. Conductivity of TCEs can be improved by incorporating metallic grids,[20–22] these can be produced by thermal evaporation using shadow masks, by lithography or by printing.[20,23] Considering that fabrication methods should be scalable and low cost, a method is proposed here to produce both PET supported and free standing metallic grids by ink-jet printing of silver nanoparticles followed by electrodeposition of copper (also other metals can be deposited depending on the application) and, optionally, electropolishing. Ink-jet printing was demonstrated to allow the production of grid electrodes with low resistivity supported on rigid substrates[24] as well as on flexible substrates like PET; combination of printed Ag meshes and graphene is also being considered.[25] Ink-jet printing of flexible patterns is advantageous since it allows depositing metal on-demand, thus reducing the amount of necessary material and therefore production costs. The main limitations of this technology are the low softening point of polymeric substrates and the minimum drop size that can be ink-jetted. The former sets an upper boundary to operating temperature during the sintering step of the process, the latter limits the minimum feature size that can be obtained with this technology. Since the dimension of metal lines of the final grid (free standing or polymer supported) has a lower limitation, determined by the initial width of the ink-jetted lines, optimization was performed in order to reduce this parameter. Dimension and shape of the ink droplet were controlled by tuning the voltage waveform acting on the piezoelectric actuator; drop distance was optimized in order to maintain metal line uniformity while reducing the feature width.

Considering also the subsequent steps of electrodeposition and electropolishing, it is possible to tune the properties of the final electrode as required, simply by properly modulating process parameters.

Experimental

Materials.— Commercial PET films, 150 μm thick, were used as substrates. Commercial Suntronic EMD5603 ink was used, supplied by SunChemical, consisting in an ethylene glycol based suspension of Silver nanoparticles (20%w/w) with diameter lower than 150 nm. G222SRAH - Commercial Acid Copper Plating solution, by Reprochem Srl. Indium tin oxide coated PET was obtained by Sigma-Aldrich and used as received. The electrolyte for electropolishing was prepared using ortho-phosphoric acid (85%, Sigma-Aldrich), potassium phosphate (monobasic KH_2PO_4 and dibasic K_2HPO_4, Sigma-Aldrich), benzotriazole (Sigma-Aldrich), and de-ionized water.

Ink-Jet printing of micronets.— Metallic grids were printed using a Dimatix Materials Printer 2831 inkjet-printer; this is equipped with a piezoelectric print-head having 16 nozzles, linearly spaced at 254 μm on a single row, with diameter 25 μm. This printer allows manipulating the waveform of electric pulses driving piezo-jetting devices. The qualitative scheme of the waveform used in the inkjet printing process is given in Figure 1; this was the result of a series of optimization tests performed with the aim of obtaining small spherical drops. The tail can indeed deflect the freefalling path and introduce bulges into

*Electrochemical Society Student Member.
**Electrochemical Society Active Member.
zE-mail: andreavittorio.oriani@polimi.it

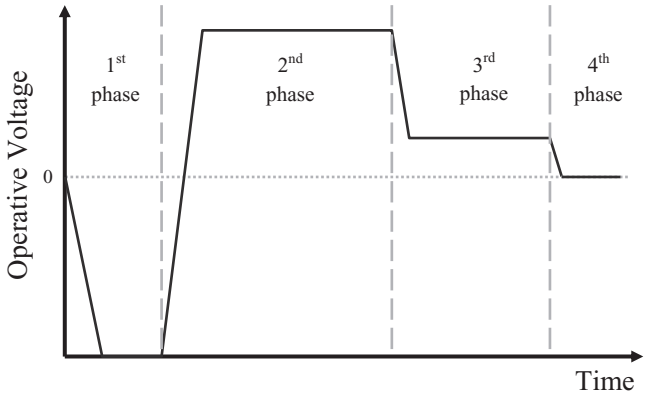

Figure 1. Qualitative scheme of the Voltage waveform used to eject the single ink drop during ink-jet printing.

the printed features, if it is not absorbed into the drop head before the latter reaches the substrate. The duration of the pump-in step, at negative voltage (1st phase), was tailored in order to induce ink flow, minimizing the volume forced into the pumping chamber. The next two phases are relative to ejection of the pre-pumped ink and drop shape definition. A high slew rate was therefore selected, in order to reduce formation of non-spherical drops. During the last phase, the driving voltage was set to zero, thus allowing the system to return to its original conditions. Metallic grids with different geometrical parameters were printed, on the PET substrate heated at 60°C, using several drop spacing values and three different operating voltages. Sintering was performed at 110°C for 60 min.

Characterization of printed micronets.— Laser profilometry was used to determine printed line spacing and thickness. An UBM microfocus instrument was used. SEM imaging was performed with a Zeiss Leo Supra 35 field emission microscope to have a deeper insight on the quality of the printed pattern.

Bending tests were done in compliance of the ISO 1519 norm, using BYK cylindrical mandrel tester ISO version. Resistivity measurements were performed, with a Keysight Technologies U1232A multimeter, on suitable rectangular samples having a continuous coating of silver at each corner, as reported in Figure 2. This geometry allows determining resistivity across both adjacent (horizontal, vertical) and opposite (diagonal) corners of the micronet pattern. Light transmission properties of the micronets were determined using Perkin Elmer Lambda 2 spectrophotometer in transmission mode, with data point spacing of 1 nm in the 190–1100 nm range. Measured values

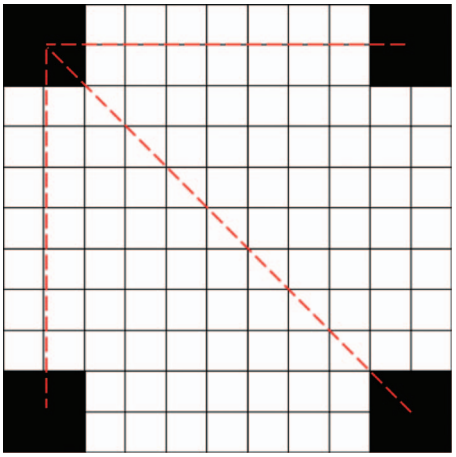

Figure 2. Schematic representation of sample geometry adopted to characterize electrical properties of the printed micronet.

Table I. Experimental conditions and electrolyte used for copper electrodeposition on printed micronets to obtain freestanding grids.

Plating Solution	G222SRAH - Commercial Copper Plating solution, Reprochem Srl
Anode	Platinum
Plating Temperature	30°C
Stirring	Magnetic @ 200 rpm
Current Density	50 mA/cm^2 (Strike), 30 mA/cm^2 (Deposition)
Deposition Time	1 min Strike, 60 min Deposition

were associated to the metallic pattern geometry and resistivity, in order to determine the best compromise between the two properties (resistivity and light transmission).

Production of freestanding meshes.— To fabricate the free standing transparent electrode, electroplating was performed on the printed pattern, using the two electrodes setup, in the conditions reported in Table I. Optionally electropolishing was performed on the free standing metallic grid to reduce metallic line dimensions. This was performed in the three electrode setup, using Platinum as counter electrode and a saturated Ag/AgCl reference electrode. A phosphoric acid based bath, described elsewhere,[26] was used to perform electropolishing in potentiostatic conditions.

Results and Discussion

Given the different properties and the different process needed to manufacture free standing and polymer supported micronets, the discussion is divided depending on the final product of the process.

Ink-Jet printing of PET supported micronets.— Considering the printing of conductive lines to produce transparent conductive electrodes, drop spacing plays a critical role. This deeply affects line width: increase in drop spacing leads to a reduced line width, therefore to higher light transmission, but at the same time this can cause issues in electrical conductivity and continuity of the array. The opposite can occur when reducing drop spacing. Figure 3 reports line width values obtained for different drop spacing and operating voltages (meant as drop ejection voltage). It can be noticed that results at 21 V and 22 V are comparable while small differences are observed at 23 V operative voltage; higher influence is played by drop spacing. Being 35 μm the average diameter of the spherical drops (as observed with the camera installed in the printer), an optimal value for drop spacing was identified as 30 μm. The influence of drop spacing on line thickness was then evaluated by laser profilometry. Several measurements, performed on samples obtained in different experimental conditions, show that no remarkable influence is exercised by this parameter on

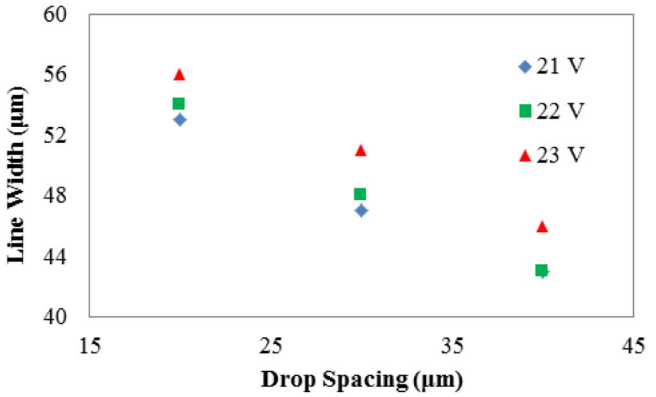

Figure 3. Graphical representation of the relationship between line width and drop spacing, reported for three values of operational voltage.

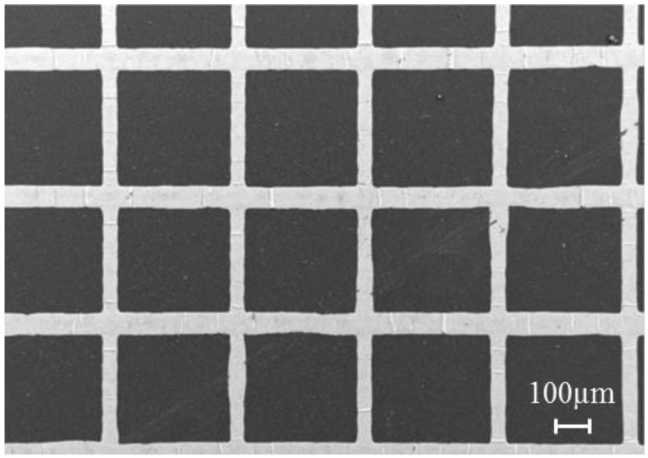

Figure 4. Scanning electron microscope image of a portion of PET supported ink-jet printed micronet.

line thickness. The same value, about 3 µm, was obtained for line thickness after sintering, independently on drop spacing. This is reasonable considering that, for a given volume of ink, drop shape does not depend on drop spacing and is directly related to wettability, i.e. contact of the ink on the substrate.

SEM imaging, performed on printed micronets, confirmed that the selected working conditions are suitable for obtaining structures with well-defined geometry and few defects (Figure 4). Specifically line spacing and width are uniform through the whole sample. Together with the absence of delamination and cracking under bending on a cylinder with 2 mm radius, this is an indication of the good quality of the printing process.

Once quality of the printing process was validated, studies needed to be sustained on the electrical and optical properties of the micronets produced. The target was obtaining a good compromise between transparency and conductivity, having flexibility as fundamental requirement. To have a first indication on the conduction properties of the printed micronet, resistance measures were performed on commercial PET/ITO, a continuous layer of printed Ag, and a printed Ag micronet. With an inter-electrode distance of 3 cm the measured values are reported in Table II. It's possible to notice that resistance is reduced of about one order of magnitude with respect to ITO. Using the setup described in the experimental section, resistance measurements were performed on samples having different geometry in terms of line spacing and width. It is possible to observe, Figure 5a, that resistance shows a stochastic behavior with respect to line spacing and seems unaffected by this parameter. On the other hand, as expected, resistance exhibits inverse proportionality with respect to line width, Figure 5b. This dualism could be explained taking into consideration the main factor that limits conductivity on the printed pattern: apparent resistance of the micronet is much higher than that of an equivalent system composed by "bulk" Silver; this can be justified by the nature of the printed lines, composed by sintered nanoparticles. The non-dependence of resistance on line spacing could agree with its dependence on line width: the factor that limits conduction could be

Table II. Resistance values measured, with an inter electrode distance of 3 cm, for different samples and compared to commercial PET/ITO.

Sample Name	Resistance Value
Commercial PET/ITO	160 Ω
PET/ Printed Ag Micronet	25 Ω
Continuous Printed Ag	10 Ω
Freestanding Micronet	2 Ω
Re-sintered Micronet	~0.1 Ω

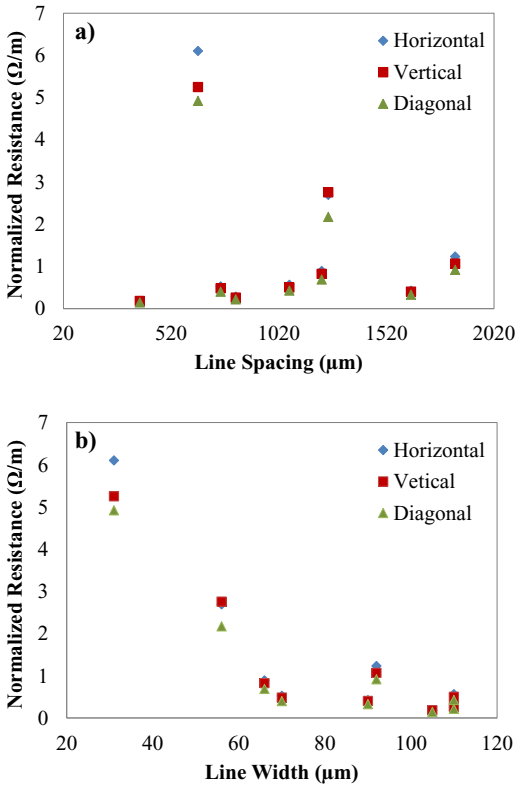

Figure 5. Graphical representation of the relationship between normalized resistance and line width (b), and normalized resistance and line spacing (a), for ink-jet printed micronets.

the presence of defects interrupting or altering the electrical continuity of the lines in the grid. The concentration of defects per unit length of printed line is roughly the same for small or large line spacing, while it is strongly increased by reduction in line width related to increase in drop spacing.

A greater impact of net geometry can be noticed on light transmission properties of the printed architecture, results are reported in Table III. Considering Sample 1, transparency measured at 550 nm is 70%, this value is slightly lower than that of the reference PET/ITO which has a measured transparency, at this wavelength, of 76%. The main parameter dominating light transmission is line spacing: an example is given comparing sample 9 and 10. With roughly the same line width, transparency at 700 nm is increased from about 43% to about 60% simply by increasing line spacing from 375 µm to 820 µm. It is

Table III. Transparency values measured at 700 nm for samples obtained with different geometrical parameters.

Sample ID #	Dimensions [µm]	Line Width [µm]	Line Spacing [µm]	Transparency [%]
1	50 × 40	31	645	71.85
2	45 × 40	38	610	69.26
3	45 × 45	56	1250	71.76
4	35 × 45	66	1220	70.35
5	45 × 45	84	1860	73.27
6	35 × 45	92	1840	71.21
7	50 × 50	60	420	55.05
8	50 × 50	90	1635	68.40
9	50 × 50	105	375	43.41
10	50 × 50	110	820	60.71
11	50 × 50	41	340	61.04
12	50 × 50	70	750	64.20
13	50 × 50	110	1070	65.06

important, when looking at the reported data, to consider that PET is responsible for part of the reduction in optical transparency and this process could be adapted to higher transparency polymers.

By correlating micronet resistance and transparency we notice the expected direct proportionality between these two characteristics. Even if optimization in terms of transparency is still needed, it is clear that line width is the main parameter governing electrical conduction while line spacing rules light transmission. Therefore depending on the requirements coming from the application it's possible to tune one or the other parameter to reach the best compromise. For example, considering results reported above, it's possible to achieve a good compromise between transparency at 700 nm in the 68%-73% range and normalized resistance, which is in the 0,5 Ω/mm-1 Ω/mm range.

Fabrication of the free standing micronet.— When considering the production of free standing transparent electrodes, mechanical performances should be considered on top of electrical conductivity and transparency. It's therefore necessary to guarantee proper stiffness for the micronet maintaining good transparency values.

The free standing transparent electrode was obtained by electrodepositing Cu on PET supported ink-jet printed micronet, but also other metals could be deposited obtaining similar results. Due to the higher adhesion of printed Ag with electrodeposited Cu than to the PET substrate, thanks to hydrogen evolution and concentration of current density at the edges of the Ag lines, self-release of the micronet was possible during the electrodeposition process. A core-shell structure is therefore obtained with this process, where electrodeposited copper completely surrounds the silver core.

Preliminary tests were performed to assess electrical resistance of the obtained freestanding micronets, with an inter-electrode distance of 3 cm; results are reported in Table II. Electrical resistance decreases of a further order of magnitude with respect to the PET supported micronet. The freestanding nature of the micronet allows performing a second thermal treatment, thus obtaining further reduction of electrode resistance (Table II). This sintering step can be performed at higher temperature with respect to the first, since no limitations are imposed by the melting temperature of PET. Electrical performances are enhanced since, on one side higher degree of coalescence is achieved among silver nanoparticles and, on the other, defects in the electrodeposited copper are reduced. Both optical and scanning electron microscopy revealed that copper coating is homogeneous on the printed pattern; moreover the original micronet geometry is maintained without alterations in line shape and distance. This confirms that deposition conditions and electrolyte allow obtaining a stress-free copper plating on the printed substrate. The mechanism of self-release is confirmed by SEM imaging performed after 30 min of Cu deposition, i.e. half of the usual plating time. It's possible to notice that copper is growing on the back side of the printed pattern but some portions of the original silver mesh are still exposed, Figure 6.

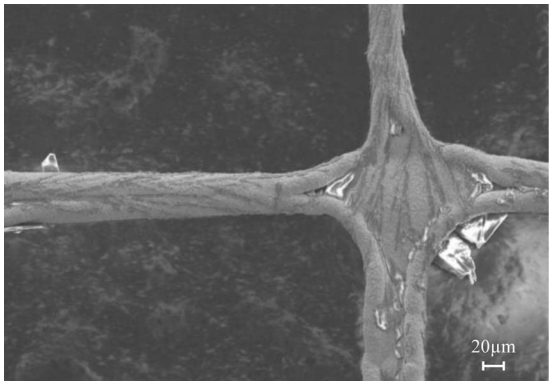

Figure 6. Scanning electron microscope image of a detail of a free standing micronet obtained after 30 min Cu electrodeposition, incomplete coverage of Ag substrate is observed.

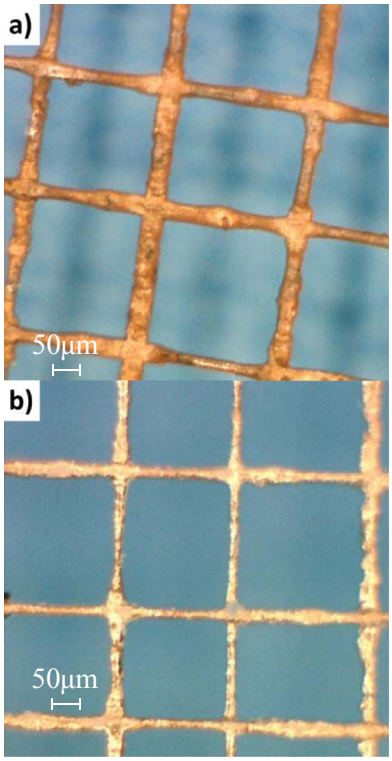

Figure 7. Optical microscope image of a free standing micronet before (a) and after (b) electropolishing, reduction in line width is observed.

This process, which on one hand allows the self-release of the freestanding micronet, on the other hand has intrinsic limitations in the amount of metal that needs to be electrodeposited to obtain a core-shell structure, with the silver substrate completely covered by copper. This can cause undesired increase in line width, leading to excessive reduction in transparency and conductivity values above the requirements. To overcome this limitation, a further step can be added to the process consisting in electropolishing. This, depending on the requirements, allows tuning line width to increase transparency in order to obtain an optimal resistivity/light transmission couple.

As revealed from optical microscopy, reduction in line width is possible by electropolishing without incurring in structural collapse or conductive track interruption. Figure 7 shows optical microscopy images of a standing micronet before and after electropolishing, while Figure 8 shows a picture of the micronet after electropolishing. It was

Figure 8. Photograph of a free standing micronet after electropolishing

possible to produce conformal geometries and to reduce line width to less than 50% of the original value, considering the average of 10 measures performed on lines randomly positioned inside the micronet.

Conclusions

It was possible to optimize ink-jet printing parameters in order to obtain PET supported micronets having a wide range of transparency and electrical conductivity values. Transparency is governed by line spacing while electrical properties are determined mainly by line width. Preliminary work was performed to produce free standing transparent electrodes by electrodeposition on printed meshes. The nature of the process leads to self-release of the freestanding electrode, which is characterized by an Ag-core Cu-shell structure. Electrode resistance can be reduced of one order of magnitude by electrodeposition; this is mainly due to the difference in microstructure between the printed Ag and the electrodeposited Cu. Sintering at higher temperature, performed on the freestanding micronet, allows to produce conformal geometries and to greatly improve electrical performances. Electropolishing can be performed to reduce line width after electrodeposition and increase transparency, maintaining acceptable electrical properties. Preliminary results obtained are encouraging. Since electrodeposition allows obtaining low resistance values even for low thickness, in the future electrodeposition could be performed on lines with reduced width in order to increase both transparency and electrical performances.

References

1. S. Reineke, F. Lindner, G. Schwartz, N. Seidler, K. Walzer, and K. Leo, *Nat. Lett.*, **459**, 234 (2009).
2. A. C. Arias, J. D. MacKenzie, I. McCulloch, J. Rivnay, and A. Salleo, *Chem. Rev.*, **110**, 3 (2010).
3. J. J. Shiang, *Interface*, **18**, 37 (2009).
4. D. R. Cairns and G. P. Crawford, *Proc. IEEE*, **93**, 1451 (2005).
5. C. Peng, Z. Jia, D. Bianculli, T. Li, and J. Lou, *J. Appl. Phys.*, **109**, 103530 (2011).
6. D. R. Cairns, R. P. Witte, D. K. Sparacin, S. M. Sachsman, D. C. Paine, G. P. Crawford, and R. R. Newton, *Appl. Phys. Lett.*, **76**, 1425 (2000).
7. S.-I. Na, S.-S. Kim, J. Jo, and D.-Y. Kim, *Adv. Mater.*, **20**, 4061 (2008).
8. M. Kaltenbrunner, M. S. White, E. D. Głowacki, T. Sekitani, T. Someya, N. S. Sariciftci, and S. Bauer, *Nat. Commun.*, **3**, 770 (2012).
9. H.-Z. Geng, K. K. Kim, K. P. So, Y. S. Lee, Y. Chang, and Y. H. Lee, *J. Am. Chem. Soc.*, **129**, 7758 (2007).
10. Z. Wu, Z. Chen, X. Du, J. M. Logan, J. Sippel, M. Nikolou, K. Kamaras, J. R. Reynolds, D. B. Tanner, A. F. Hebard, and A. G. Rinzler, *Science*, **305**, 1273 (2004).
11. T. J. Marks, *Nano Lett*., **6**, 2472 (2006).
12. S. Bae, H. Kim, Y. Lee, X. Xu, J.-S. Park, Y. Zheng, J. Balakrishnan, T. Lei, H. R. Kim, Y. Il Song, Y.-J. Kim, K. S. Kim, B. Ozyilmaz, J.-H. Ahn, B. H. Hong, and S. Iijima, *Nat. Nanotechnol.*, **5**, 574 (2010).
13. S. Jung, S. Lee, M. Song, D.-G. Kim, D. S. You, J.-K. Kim, C. S. Kim, T.-M. Kim, K.-H. Kim, J.-J. Kim, and J.-W. Kang, *Adv. Energy Mater.*, **4**, 1300474 (2014).
14. Z. Yu, Q. Zhang, L. Li, Q. Chen, X. Niu, J. Liu, and Q. Pei, *Adv. Mater.*, **23**, 664 (2011).
15. T.-H. Han, Y. Lee, M.-R. Choi, S.-H. Woo, S.-H. Bae, B. H. Hong, J.-H. Ahn, and T.-W. Lee, *Nat. Photonics*, **6**, 105 (2012).
16. L. Hu, H. S. Kim, J.-Y. Lee, P. Peumans, Y. Cui, and S. Nanowire, *ACS Nano*, **4**, 2955 (2010).
17. J.-Y. Lee, S. T. Connor, Y. Cui, and P. Peumans, *Nano Lett*., **10**, 1276 (2010).
18. W. Gaynor, J. Lee, and P. Peumans, *ACS Nano*, **4**, 1 (2010).
19. X.-Y. Zeng, Q.-K. Zhang, R.-M. Yu, and C.-Z. Lu, *Adv. Mater.*, **22**, 4484 (2010).
20. R. Søndergaard, M. Hösel, D. Angmo, T. T. Larsen-Olsen, and F. C. Krebs, *Mater. Today*, **15**, 36 (2012).
21. W.-I. Jeong, J. Lee, S.-Y. Park, J.-W. Kang, and J.-J. Kim, *Adv. Funct. Mater.*, **21**, 343 (2011).
22. S. Choi, W. J. Potscavage, and B. Kippelen, *J. Appl. Phys.*, **106**, 054507 (2009).
23. Y. Galagan, B. Zimmermann, E. W. C. Coenen, M. Jørgensen, D. M. Tanenbaum, F. C. Krebs, H. Gorter, S. Sabik, L. H. Slooff, S. C. Veenstra, J. M. Kroon, and R. Andriessen, *Adv. Energy Mater.*, **2**, 103 (2012).
24. J.-A. Jeong, S.-B. Kang, and H.-K. Kim, *J. Korean Phys. Soc.*, **63**, 62 (2013).
25. Y. H. Kahng, M.-K. Kim, J.-H. Lee, Y. J. Kim, N. Kim, D.-W. Park, and K. Lee, *Sol. Energy Mater. Sol. Cells*, **124**, 86 (2014).
26. K. G. Shattuck, J.-Y. Lin, P. Cojocaru, and A. C. West, *Electrochim. Acta*, **53**, 8211 (2008).